



25 resolution in the precision plane is - as expected - independent of the local  
26 track angle  $\phi$  within an uncertainty of  $16 \mu\text{m}$ .

27 The projected particle identification (PID) performance for a GridPix  
28 Pixel TPC in the proposed ILD experiment at a future ILC  $e^+e^-$  collider  
29 is presented using the  $B=1$  T test beam results for the measured electron  
30 PID resolution. The expected pion-kaon PID separation for momenta in the  
31 range of 2.5-45 GeV/c at  $\cos\theta = 0$  is more than  $5.5(4.5)\sigma$  for the template  
32 fit ( $dE/dx$  truncation) method.

33 *Keywords:* Micromegas, gaseous pixel detector, micro-pattern gaseous  
34 detector, Timepix, GridPix, pixel time projection chamber

---

## 35 1. Introduction

36 As a step towards a Pixel Time Projection Chamber for a future collider  
37 experiment [1], [2], a module consisting of 32 GridPix chips based on the  
38 Timepix3 chip was constructed. The GridPix chips have a very fine granu-  
39 larity of  $256 \times 256$  pixels of  $55 \times 55 \mu\text{m}^2$  and a high efficiency of about 85% to  
40 detect single ionisation electrons.

41 The 32-GridPix chip detector was put in a test beam at DESY and com-  
42 plemented with two sets of Mimosas26 silicon detector planes. The analysed  
43 data were taken at electron beam momenta of 5 and 6 GeV/c and at magnetic  
44 fields of 0 and 1 T.

45 A description of the construction of the GridPix TPC module, the test  
46 beam setup and data taking conditions can be found in part I of our paper  
47 [3], which explains the track reconstruction procedure and the precise TPC  
48 tracking results that were obtained.

49 In the following sections the analysis results for different topics will be  
50 presented. Firstly, the particle identification performance using  $dE/dx$  or  
51  $dN/dx$  will be measured. Secondly, the single-electron efficiency at high hit  
52 rates will be determined. Thirdly, the characterisation of large hit bursts  
53 caused by highly ionising particles will be presented. Fourth, the resolution  
54 in the precision plane as a function of the local track angle will be measured.  
55 Finally, the projected particle identification performance for a Pixel TPC in  
56 the proposed ILD experiment at ILC [4] will be presented and discussed.

## 57 **2. Particle Identification (PID) using $dE/dx$ or $dN/dx$**

58 Particles can be identified by their characteristic energy loss per unit  
59 of track length,  $dE/dx$  loss and/or the number of primary clusters,  $dN/dx$   
60 produced along the track. In a GridPix detector one can measure both the  
61 number of hits produced along the track and their relative distance.

62 The distribution of the number of TPC track hits per chip for the  $B = 0$   
63 T and for the  $B = 1$  T data sets are a starting point for a measurement of  
64 the  $dE/dx$  or  $dN/dx$  performance. As was discussed in part I of the paper  
65 [3], the mean number of hits per chip were measured to be 124 and 89 in  
66 the  $B = 0$  T and 1 T data sets respectively. The most probable values are  
67 respectively 87 and 64.

68 In order to measure the track performance of  $dE/dx$  or  $dN/dx$ , a track  
69 selection was applied selecting tracks crossing the central chips - defined in [3].  
70 The individual chips were calibrated to give the same mean number of hits  
71 per chip. By combining the hits associated to the track from several events,  
72 a new 1 m long track was formed. The 1 m long track has a coverage of 60%

73 because inactive regions (chip edges and e.g. guard plate) were included.

74 By applying different analysis methods, the  $dE/dx$  or  $dN/dx$  resolution  
75 can be measured from data.

76 Both methods project the hits along the track in the  $xy$  plane. This gives  
77 a distribution of hits as a function of the distance along the track in pixel  
78 units. The first method rejects large multi-electron clusters with more than  
79 in total 6 hits in 5 consecutive pixel bins. Finally, a  $dE/dx$  truncation at 90%  
80 is performed using samples of 20 pixels; so the 10% largest  $dE/dx$  values are  
81 removed and  $dE/dx$  re-estimated. This method does not fully exploit the  
82 full granularity of the pixel TPC.

83 The second method exploits the distribution of the minimum distance  
84 between consecutive hits in the  $xy$  precision plane. If only single-electron  
85 clusters were produced in a gas, one would expect an exponentially falling  
86 distance distribution. Multi-electron clusters will give rise to a peak at low  
87 distances that is smeared out by the transverse diffusion process. The slope  
88 of the exponential distribution is proportional to the  $dN/dx$  i.e. the clusters  
89 produced by the traversing beam electron. The long Landau tail in the  
90  $dE/dx$  distribution is coming from the multi-electron clusters that will peak  
91 at low distances.

92 Using a large number of tracks, it is possible to measure from data the  
93 shape of the minimum distance distribution. At distances above approxi-  
94 mately 10 pixels the distribution follows an exponential distribution - see  
95 Fig 5.19 in [2]. At lower distance, weights for the  $B=0$  T and 1 T data are  
96 determined and applied to ensure an exponential distribution over the whole  
97 range.

98 Finally, per 1 m of track length, a fit to the distance distribution in data  
99 is performed with the following template function:

$$N(d_{xy}) = N_0 \text{weight}(d_{xy}) e^{-\alpha \cdot d_{xy}}, \quad (1)$$

100 where  $d_{xy}$  is the minimum distance of the hits in the precision plane ( $xy$ ).  
101 The slope  $\alpha$  and  $N_0$  - normalisation - are left free in the per track fit. The  
102 weights for the  $B = 0$  and 1 T data are fixed using the whole data set.

103 The test beam data provide a  $dE/dx$  or  $dN/dx$  measurement for electrons.  
104 The data were also used to perform a measurement of the response of a  
105 minimum ionising particle (MIP) - here defined as a particle that produced  
106 70% of the electron  $dE/dx$ . By dropping 30% of the hits associated to the  
107 track and applying the two methods, the response of a MIP was measured  
108 and the linearity of the methods tested.

109 The relative resolution is defined as the r.m.s. of the distribution divided  
110 by the mean and the results are shown in Table 1. The resolution of the  $B =$   
111 1 T data is about 40% better than the  $B = 0$  T data. This is consistent with  
112 the smaller fluctuations that are present in the distributions of the number  
113 of hits per chip in the  $B = 1$  T data [3]. The template fit method has in the  
114  $B = 1$  T data a 20% better performance than the  $dE/dx$  truncation method.  
115 One might argue that with more diffusion the results from the template fit  
116 method will move more towards the results of the  $dE/dx$  truncation method.  
117 Note however that the diffusion contribution to the track resolution in the  
118 1 T data is already sizeable compared to the pixel size and varies between  
119 85-150  $\mu\text{m}$ .

120 The results for the 1 T data are shown in Fig. 1, for electrons and MIPs  
121 and for the  $dE/dx$  truncation and template fit methods. The unit of the

Table 1:  $dE/dx$  or  $dN/dx$  relative resolution for different methods and data sets

Method	$B=0$ T	$B=1$ T
$dE/dx$ truncation	6.0 %	3.6 %
template fit	5.4 %	2.9 %

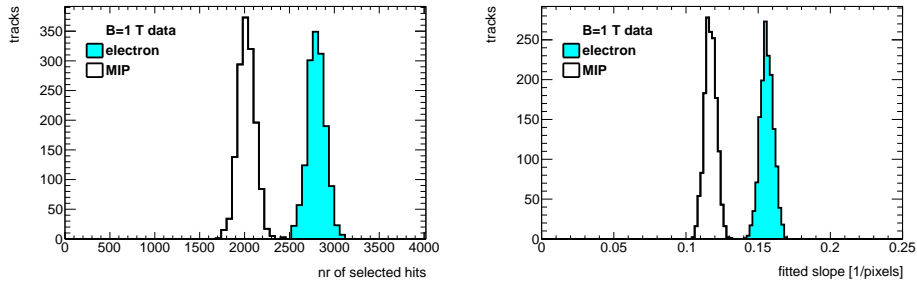


Figure 1: Distribution of the number of selected hits per track for the  $dE/dx$  truncation method (left) and the fitted slope for the template fit method (right) for an electron (light blue shaded) and for a MIP, using 1 m long tracks with 60% coverage, for the  $B = 1$  T data.

122 fitted slope is inverse pixel, as is clear from the formula in Eq. 1. The  
 123 linearity - defined as the mean MIP response divided by the mean electron  
 124 response divided by 0.7 - was measured to be 1.03 for method 1 and 1.07 for  
 125 the template fit method. This value is slightly different from 1, and can be  
 126 corrected by scaling the expected values for different particles as a function  
 127 of the measured momentum.

128 The  $dE/dx$  or  $dN/dx$  result of the 32-chip GridPix detector for electrons  
 129 is impressive. It has currently, the best resolution per meter of track length  
 130 of constructed TPCs running at atmospheric pressure - and demonstrates  
 131 the particle identification (PID) capabilities of a GridPix Pixel TPC.

132 **3. Single-electron efficiency at high hit rates**

133 The efficiency of the GridPix device to detect a hit in a high (low) rate  
 134 environment is measured comparing the mean time over threshold (ToT) for  
 135 low and high rate runs at B fields of 0 and 1 T. The mean ToT is sensitive  
 136 to the single-electron efficiency of the detector. In order to extract a precise  
 137 result, hits associated to TPC tracks were used. The track selection is the  
 138 same as in section 2. The analysed runs for the  $B = 0$  T data set were runs  
 139 6916, 6934 and 6935 and for the  $B = 1$  T data set runs 6969 and 6983.

140 For each run the mean ToT values were measured in the interval between  
 141 0.15 and 1.4  $\mu$ s. These cuts were applied to remove the noise and the upper  
 142 tail of the distribution.

Table 2: Measured mean ToT and rates for different runs

run	B	ToT1	ToT2	triggers	run time	Hits1	Hits2	trig rate	Rate1	Rate2
	[T]	[ $\mu$ s]	[ $\mu$ s]	$10^3$	[ $10^3$ s]	$10^6$	$10^6$	[Hz]	[ $10^3$ hits/s]	[ $10^3$ hits/s]
6916	0	0.628	0.653	16.8	5.81	6.25	13.1	2.9	1.08	2.26
6934	0	-	0.651	73.4	0.60	-	20.5	121.7	-	33.92
6935	0	0.620	-	73.9	0.60	6.95	-	122.5	11.51	-
6969	1	0.650	0.666	7.94	3.45	1.93	2.16	2.3	0.56	0.62
6983	1	0.657	0.678	67.9	0.70	11.6	14.1	96.2	16.44	19.94

143 The results for the measured average ToT for different runs and hit  
 144 rates are summarised in Table 2. ToT1(2) denotes the mean ToT for upper  
 145 and lower half (in  $x$ ) of the module and Hits1(2) corresponds to number of  
 146 recorded raw hits. The number of triggers and trigger rate are not corrected

147 for the trigger efficiency of about 31%. The mean Rate1(2) was calculated  
 148 dividing the total number of raw hits by the total run time. The instant-  
 149 neous rate in runs 6934, 6935 and 6983 taken at 5 GeV/c is about a factor  
 150 3 higher (due to the duty cycle of the machine). For the  $B = 0$  T data, two  
 151 high rate runs 6934 and 6935 taken at a beam momentum of 5 GeV/c had  
 152 to be analysed because the beam crossed either the upper or the lower part  
 153 of the module and therefore no measurement could be performed in one of  
 154 the parts (denoted by -). The statistical uncertainties are negligible.

155 The relative change in the mean ToT for the  $B = 0$  data is -1.3% (upper  
 156 half) and -0.3% (lower half). In this case the rate goes up to 34 kHz for 6  
 157 chips or 5.7 kHz per chip. The relative change in the mean ToT for the  $B =$   
 158 1 T data is +1.1% (upper half) and +1.8% (lower half) The rate goes up to  
 159 20 kHz for 6 chips or 3.3 kHz per chip.

160 The relative change in the mean ToT can be related to the relative change  
 161 in the single-electron efficiency  $\delta\epsilon/\epsilon$  by:

$$\delta\text{ToT}/\text{ToT} = d \delta\epsilon/\epsilon. \quad (2)$$

162 The derivative  $d$  is about 0.5 at the mean working point of  $\text{ToT}=0.65 \mu\text{s}$  and  
 163 is determined from the measured efficiency-ToT curve in Fig. 4.7 of [2].

164 This means that the relative efficiency is stable at the level of +0.9% ( $B$   
 165 = 1 T) and -0.6% ( $B = 0$  T) for hit rates up to 3.3 (5.7) kHz per chip. To  
 166 conclude, running at hit rates up 5.7 kHz per chip gives a reduction of at  
 167 most 0.6% in the relative efficiency.



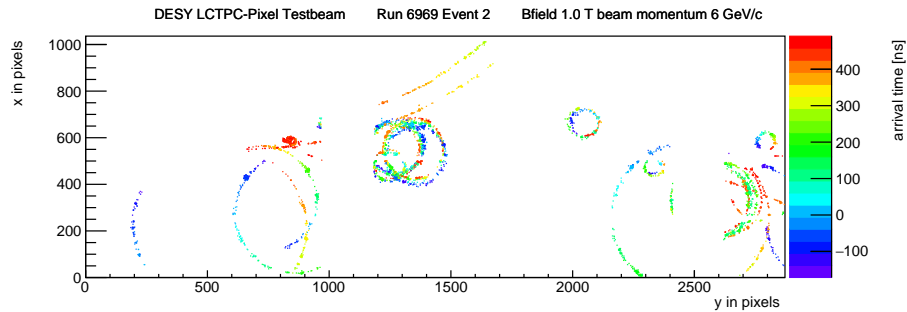


Figure 2: An event display for run 6969 event 2 taken at a 5 GeV/c beam momentum in a  $B = 1$  T field. The hits are shown in the  $xy$  plane, in colour the time of arrival is shown.

#### 168 4. Characterisation of hit bursts

169        In event displays hit burst caused by highly ionising particles (e.g. alpha  
 170 particles or delta electrons) can be observed. An example event is shown in  
 171 Fig. 2. A large variety of hit patterns can be observed: large radii (open)  
 172 circles, smaller size radius circles from low momentum particles, curlers and  
 173 more confined bursts. A track with a momentum of 1 MeV/c will have a  
 174 typical radius of 60 pixels. A Pixel TPC is well suited to study and charac-  
 175 terise these typical hit bursts. After a reconstruction and characterisation of  
 176 the burst it is possible to reject the hits associated to the bursts. This will  
 177 improve the measurement of the track parameters in the final track fit.

178        To study the hit bursts, the data of run 6969 - taken at a 5 GeV/c beam  
 179 momentum in a  $B = 1$  T field - were analysed. Bursts were selected with  
 180 more than 100 hits in a radius of 50 pixels around the burst centre within  
 181 a time window of 200 ns around the mean time. The mean position in  $xy$   
 182 and the mean time of the burst were iteratively estimated. The bursts were  
 183 characterised by the number of associated hits, the radius in which 90% of the

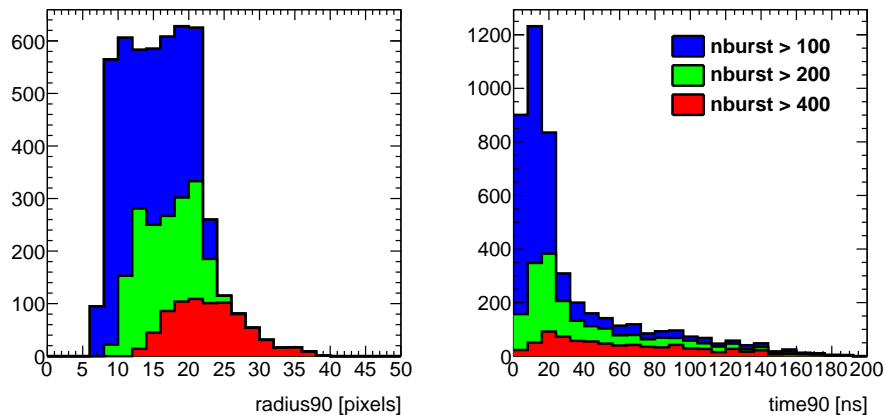


Figure 3: The stacked distributions for radius90 and time90, for bursts with more than 100 (blue), 200 (green) and 400 (red) hits, in run 6969.

184 hits are found (radius90) and the time in which 90% of the hits are detected  
 185 (time90). The stacked distributions for the radius90 and time90 variables for  
 186 different burst sizes are shown in Fig. 3.

187 It is clear that the radius90 and time90 distributions broaden as a function  
 188 of the number of hits. In particular the time90 distribution develops a long  
 189 tail for high number of hits. Note that hits that end up on the same pixel  
 190 within the Timepix3 pixel dead time of 475 ns will not be recorded, so part  
 191 of the core of the burst may remain undetected. Still, the detector is able to  
 192 record hit bursts of at most 7854 hits in a 50 pixel radius. The largest hit  
 193 burst in the run used in Fig. 3 had 3180 hits.

194 For high momentum tracking it is important to cut tightly on the track  
 195 residuals in  $xy$  and  $z$ . In particular the cut in  $z$  reduces the impact of bursts  
 196 in the  $B = 1$  T data. Therefore in future pattern recognition software one  
 197 could run a burst finding algorithm and down weight in the track fit the

198 hits associated to bursts. This will remove biases and improve the track  
199 parameter estimation.

## 200 **5. Track resolution as function of the local track angle**

201 The resolution in the precision plane as a function of the local track angle  
202 will be measured in the  $B = 1$  T data set. For a pad based readout system  
203 the resolution has a strong dependence on the local track angle see e.g. [5].  
204 The resolution is best if the local track angle is parallel to the strip direction.

205 For a GridPix pixel TPC - with squared pixels - the resolution is expected  
206 to be independent of the local track angle. In order to test experimentally  
207 this hypothesis, reconstructed circle tracks were selected. Examples of circle  
208 tracks can be observed in the event display shown in Fig. 2. For circles,  
209 the local track angle  $\phi$  depends on the position of the individual hits on the  
210 circle in the  $xy$  plane. The range of  $\phi$  angles depends on the radius. For radii  
211 smaller than 500 pixels a large  $\phi$  range can be probed. Using the residuals in  
212 the  $xy$  plane, it is possible to measure the resolution of the hits as a function  
213 of the local track angle.

214 A dedicated pattern recognition program was written to find and fit mul-  
215 tiple circles in an event. To find candidate circles, a Hough transform was  
216 used to find the centre of the circle in the  $xy$  plane. In the circle fit, the reso-  
217 lution in  $xy$  was estimated to be about 4 pixels and in  $z$  it was 1 mm. Outlier  
218 hits at more than 2.5 standard deviation were iteratively rejected. For the  
219 selection of circles it was required that the fit  $\chi_{xy}^2/d.o.f.$  and  $\chi_z^2/d.o.f.$  were  
220 less than 5. Finally, the radius of the circle had to be larger than 50 pixels  
221 (corresponding to a momentum cut of 0.8 MeV/c) and at least 20 hits should

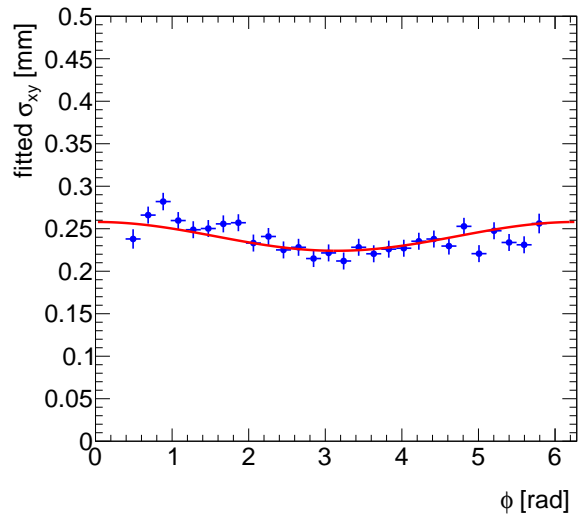


Figure 4: The fitted resolution in  $xy$  as a function of the local track angle  $\phi$  for the hits on the circle. The fitted curved in red is given in Eq. 3.

222 lie on the circle. The total  $\phi$  span of the selected hits on the circle should be  
 223 at least 1 rad. The hits with local  $\phi$  values below  $\pi/8$  and above  $15\pi/8$  were  
 224 removed.

225 The selected data set has 973 circles, with a mean radius of 155 pixels  
 226 and a mean number of hits of 194. Because the resolution depends on the  
 227 radius (i.e. the momentum) and small radii span a large  $\phi$  range, the data  
 228 were re-weighted as a function of the circle radius. Finally, the resolution in  
 229  $xy$  was extracted - using a Gaussian fit to the track residuals in the range of  
 230  $\pm 2\sigma$  around the centre. The fitted resolution in  $xy$  as a function of the local  
 231 track angle  $\phi$  for the hits on the circle is shown in Fig. 4.

232 A curve was fitted to the data using the following expression:

$$\sigma_{xy} = \sigma_0 + \sigma_1 \cos \phi, \quad (3)$$

233 where  $\sigma_0$  and  $\sigma_1$  were left free. The fit result yielded  $\sigma_0 = 0.241$  mm and  
 234  $\sigma_1 = 0.016$  mm and describes the modulation observed in the data.

235 It can therefore be concluded that the resolution in the precision plane is  
 236 independent of the local track angle  $\phi$  within an uncertainty of  $16 \mu\text{m}$ .

237 *5.1. Projected particle identification performance for a Pixel TPC in the pro-*  
 238 *posed experiment ILD at a future ILC*

239 The particle identification (PID) performance of electrons in the test  
 240 beam for momenta of 5-6 GeV/c was measured to be 2.9% for the tem-  
 241 plate fit and 3.6% for the  $dE/dx$  truncation method at  $B = 1$  T for 1 m long  
 242 tracks with 60% coverage. The TPC of the proposed ILD detector [4] has  
 243 an inner radius of 329 mm, an outer radius of 1770 mm and a half length  
 244 of 2350 mm. The expected electron PID resolution in the ILD TPC is then  
 245 expected to be 2.4% (template fit) and 3% (truncation method) at polar an-  
 246 gles of  $\theta = \pi/2$  ( $\cos \theta = 0$ ) and a track length ( $\text{tlength}_0$ ) of 1441 mm. The  
 247 PID resolution for different particles can be written as:

$$\sigma_i = \sigma_e \sqrt{\text{tlength}_0 \cdot E_e / \sqrt{\text{tlength} E_i}}, \quad (4)$$

248 where  $\text{tlength}$  is the track length and  $E_i$  is the expected energy loss for  
 249 particle  $i$  (electron =  $e$ , muon =  $\mu$ , pion =  $\pi$ , kaon =  $K$ , proton =  $p$ ).  
 250 Clearly, the best PID resolution will be reached for the largest track length,  
 251 which corresponds to  $\cos \theta = 0.85$  in ILD.

252 The ILD parametrisations of the energy loss for different particles as a  
 253 function of the momentum were used as given in [6]. They are based on  
 254 full simulations of the ILD TPC operated with a T2K gas and running at  
 255 atmospheric pressure. The PID separation in numbers of standard deviations

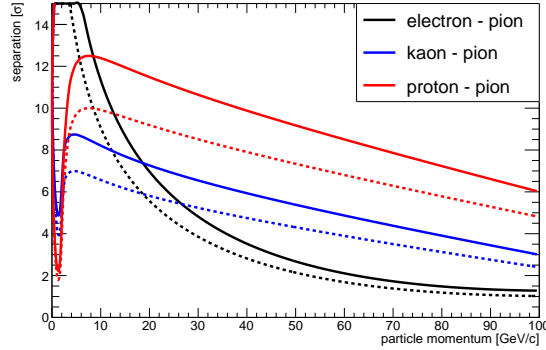


Figure 5: The projected PID separation for a GridPix TPC in ILD for electrons, kaons and protons w.r.t. pions at  $\cos\theta = 0$ . The continuous lines correspond to an electron PID resolution of 2.4% and the dashed to 3%.

256 w.r.t. the  $\pi$  hypothesis for  $e$ ,  $K$  and  $p$  are defined as:

$$\text{PID separation}_i = |E_i - E_\pi|/\sigma_\pi. \quad (5)$$

257 In Fig. 5, the separation of electrons, kaons and protons w.r.t. pions are  
 258 shown as a function of the momentum of the particle, for the projected ILD  
 259 electron PID resolutions of 2.4 and 3% at  $\cos\theta = 0$ . The expected pion-kaon  
 260 PID separation for momenta in the range of 2.5-45 GeV/c at  $\cos\theta = 0$  is  
 261 more than  $5.5(4.5)\sigma$  for the two resolution scenarios. At a momentum of  
 262 100 GeV/c the separation is still  $3.0(2.0)\sigma$ . Protons can be separated from  
 263 pions for momenta in the range of 2.5-100 GeV/c with more than  $6.0(4.8)\sigma$ .

264 It is clear from the above that a GridPix Pixel TPC in ILD will provide  
 265 powerful particle identification.

## 266 6. Conclusions and outlook

267 A Time Projection Chamber (TPC) module with 32 GridPix chips was  
268 constructed and the performance was measured using data taken in a test  
269 beam at DESY in 2021. The analysed data were taken at electron beam  
270 momenta of 5 and 6 GeV/c and at magnetic fields of 0 and 1 T.

271 The precise tracking results for the module were presented in part I of  
272 the paper [3].

273 The  $dE/dx$  or  $dN/dx$  resolution for electrons of momenta 5 and 6 GeV/c  
274 in the 1 T data for a 1 m long track with 60% coverage was measured to be  
275 3.6% for the  $dE/dx$  truncation method and 2.9% for the template fit method.  
276 This result is impressive and is currently the best PID resolution per meter  
277 of track length of constructed TPCs running at atmospheric pressure.

278 The single-electron efficiency at high hit rates was studied. For hit rates  
279 up 5.7 kHz per chip a reduction of at most 0.6% in the relative efficiency was  
280 measured.

281 Hit bursts due to highly ionising particles were characterised showing the  
282 pattern recognition capabilities of a GridPix Pixel TPC.

283 The resolution in the precision plane as a function of the local track angle  
284 was measured in the  $B = 1$  T data using reconstructed circle tracks. It was  
285 demonstrated that the resolution in the precision plane is - as expected -  
286 independent of the local track angle  $\phi$  within an uncertainty of 16  $\mu\text{m}$ .

287 The projected particle identification performance for a GridPix Pixel TPC  
288 in ILD was presented using the  $B = 1$  T test beam results for the measured  
289 electron PID resolution. The expected pion-kaon PID separation for mo-  
290 menta in the range of 2.5-45 GeV/c at  $\cos\theta = 0$  is more than 5.5 (4.5)  $\sigma$  for

291 the template fit ( $dE/dx$  truncation) method.

292 It is clear that a GridPix Pixel TPC in ILD will provide powerful parti-  
293 cle identification. At the CEPC collider a Pixel TPC is proposed, because  
294 of the precise tracking and particle identification capabilities. The GridPix  
295 detector will be further tested and developed for a TPC that could be in-  
296 stalled in a heavy ion experiment at the Electron Ion Collider. In the DRD1  
297 collaboration at CERN a GridPix Pixel TPC is also part of the research  
298 program.

## 299 **Acknowledgments**

300 This research was funded by the Netherlands Organisation for Scientific  
301 Research NWO. The authors want to thank the support of the mechanical  
302 and electronics departments at Nikhef and the detector laboratory in Bonn.  
303 The measurements leading to these results have been performed at the Test  
304 Beam Facility at DESY Hamburg (Germany), a member of the Helmholtz  
305 Association (HGF).

## 306 **References**

- 307 [1] M. Lupberger, Y. Bilevych, H. Blank, D. Danilov, K. Desch, A. Hamann,  
308 J. Kaminski, W. Ockenfels, J. Tomtschak, S. Zigann-Wack, To-  
309 ward the Pixel-TPC: Construction and Operation of a Large Area  
310 GridPix Detector, IEEE Trans. Nucl. Sci. 64 (5) (2017) 1159–1167.  
311 doi:10.1109/TNS.2017.2689244.
- 312 [2] C. Ligtenberg, A GridPix TPC readout for the ILD experiment at the  
313 future International Linear Collider, Ph.D. thesis, Free University of



- 314 Amsterdam (2021).  
315 URL [https://www.nikhef.nl/pub/services/biblio/theses\\_pdf/thesis\\_C\\_Ligtenberg.p](https://www.nikhef.nl/pub/services/biblio/theses_pdf/thesis_C_Ligtenberg.p)
- 316 [3] M. van Beuzekom, et al., Towards a Pixel TPC part I: construction and  
317 test of a 32-chip GridPix detector, submitted to Nucl. Instrum. Meth.  
318 A.
- 319 [4] T. Behnke, J. E. Brau et al., eds. The International Linear Collider.  
320 Technical Design Report. Vol. 4: Detectors. Linear Collider Collabora-  
321 tion, 2013. arXiv: 1306.6329. doi:10.48550/arXiv.1306.6329.  
322 URL <https://www.linearcollider.org/>
- 323 [5] LCTPC Collaboration, David Attié et al., A Time Projection Cham-  
324 ber with GEM-Based Readout, Nuclear Instruments and Methods in  
325 Physics Research. Section A: Accelerators, Spectrometers, Detectors  
326 and Associated Equipment 856, 1 (2017), 109–118. arXiv:1604.00935v1,  
327 doi:10.1016/j.nima.2016.11.002.
- 328 [6] iLCSoft, Linear Collider Software,  
329 URL <https://github.com/iLCSoft/MarlinReco/blob/master/Analysis/PIDTools/>,  
330 based on version v02-02-01.